

The instrumental record of ENSO: 1840s – 2000

Todd P. Mitchell and John M. Wallace

Stanley P. Hayes Center for the Study of Climate Variability
Joint Institute for the Study of the Atmosphere and Ocean (JISAO)
University of Washington

Submitted to the Journal of Climate on

1 October 2001

A PDF file for this manuscript is available at:

http://jisao.washington.edu/wallace/enso_chronology.pdf

Corresponding Author: Todd Mitchell, JISAO, Box 354235, University of Washington, Seattle
WA, 98195-4235; mitchell@atmos.washington.edu

Abstract

ENSO variability in the tropics from the late 19th century onward is documented, making use of three indices: sea surface temperature averaged over the central and eastern equatorial Pacific minus global-mean sea surface temperature; the sea-level pressure anomaly averaged over the eastern Indian Ocean; and a multivariate index constructed from sea-level pressure, surface winds, and rainfall anomalies over the tropics. These three ENSO indices vary synchronously on seasonal to annual time scales from 1870 onward, and on decadal time scales from the 1890s onward. With few minor exceptions (largely in the extratropics) the structure of ENSO-related anomalies in global wind, temperature and precipitation fields has changed very little since the late 19th century. Nor is there convincing visual evidence of secular trends or changes in the frequency or amplitude of warm or cold episodes of the ENSO cycle.

1. Introduction

The decade of the 1990's began with an extraordinarily long warm episode of the El Niño / Southern Oscillation (ENSO) cycle; it witnessed an extraordinarily strong one-year warm episode (1997-98); and it ended with the most protracted cold episode in several decades. Whether this behavior was truly extraordinary in the context of the long term historical record of ENSO has been subject to debate (Trenberth and Hoar 1996; Harrison and Larkin 1997; Rajagopalan et al. 1997, 1999; Allan and D'Arrigo 1999; Trenberth and Hurrell 1999a,b; and Wunsch 1999a,b). The controversy has motivated a number of recent efforts to extend the historical record of the ENSO cycle backward into the late 19th century. Notable among the products of these efforts are Darwin and Tahiti sea-level pressure (SLP) anomaly time series derived from blended marine and land observations by Basnett and Parker (1997) and from marine observations by Kaplan et al. (2000), an extension of the Djakarta SLP record by Können et al. (1998), an equatorial Pacific sea surface temperature (SST) anomaly index by Trenberth and Stepaniak (2001), and the development of ENSO proxies from merged Java and U.S. tree rings by Stahle et al. (1998) and western equatorial Pacific corals by Urban et al. (2000).

The present contribution compliments these historical reconstructions by documenting the time history of the ENSO cycle based on three different indices: 1) an unsmoothed monthly equatorial Pacific SST index analogous to NINO-3 (Rasmusson and Carpenter 1982), but calculated as a departure from the current anomaly in global-mean SST; 2) a lightly smoothed pressure index based on long station records in the western lobe of the Southern Oscillation, analogous to indices of Walker and Bliss (1932, 1937) and Berlage (1966); and 3) a multivariate dynamical index based on wind, pressure, and rainfall data.

These time series (as well as the individual constituents of the dynamical index) exhibit a consistent sequence of year-to-year variability from 1920 onward. The degree to which such consistency prevails during World War I and farther backward into the 19th century provides a measure of the credibility of the more extended time series and the statistics derived from them.

The interpretation of ENSO-related variability in extended historical records is complicated by the existence of global warming. Defining warm and cold episodes of the ENSO cycle in terms of fixed thresholds for equatorial Pacific SST anomalies relative to a single climatology imposes a bias toward cold episodes in the earlier part of the record and warm episodes in the later part. Fedorov and Philander (2000) limited this trend by defining ENSO-related anomalies relative to a time-varying climatology based on a 11-year low-pass filter. In our analysis it is largely eliminated by removing the global-mean SST anomaly for each year and month.

Current conceptions of global spatial patterns and seasonality of ENSO-related variability are largely based on analyses of data for the second half of the 20th century. Thanks to the data set development efforts of the past 20 years, the information on year-to-year climate variability during the earlier part of the historical record is now sufficiently reliable to support a preliminary assessment of the structure and seasonality of ENSO as far back as the middle of the 19th century. This paper contrasts linear regression patterns of SLP, surface wind, SST, surface air temperature (SAT), and precipitation based on the equatorial Pacific SST index for the periods of record 1854-99, 1900-49, and 1950-2000. It also compares the seasonality of selected ENSO indices during these same three periods.

The paper is organized as follows. The next section provides essential technical information on data sources and preliminary data processing. Section 3 describes the indices and how they are constructed and compares them with previously published indices. Section 4 compares extended time series of the three indices. Section 5 contrasts the spatial structure of ENSO-related variability during the late 19th century and the first and second halves of the 20th century. The final discussion section offers a brief assessment of ENSO-related variability in the historical record based on the evidence presented in this paper.

2. Data sets and preliminary processing

The gridded data sets employed in this study and the periods of record used in individual analyses are listed in Table 1. The Lamont-Doherty Earth Observatory (LDEO) SSTs (Kaplan et al. 1997, 1998) and SLPs (Kaplan et al. 2000) are optimal smoothing and optimal interpolation analyses, respectively, in which the structure functions are derived from covariance statistics based on the recent record. Regression maps produced from the LDEO data sets are qualitatively similar to those obtained from the United Kingdom Meteorological Office Global Mean Sea Level Pressure data set (Tracy Basnett 1999, personal communication) and lightly (spatially) smoothed Comprehensive Ocean-Atmosphere Data Set (COADS; Woodruff 2001a,b) anomalies for the same periods (not shown). The analyses derived from the LDEO data are used as a basis for the regression maps in this study because they are somewhat easier to contour than their COADS-based counterparts.

All of the gridded data sets were processed in the following manner. A climatological mean was calculated for each field and calendar month for 1950-79, a well-sampled period with relatively little interdecadal variability. The climatologies for the 2° latitude-longitude resolution COADS fields were subjected to successive five- and three-point running mean smoothers along latitude circles. Filtering was performed only along latitude circles in order to preserve the smallest resolvable meridional scales of the equatorial features. The climatological mean fields were subtracted from the original data to produce anomaly fields.

COADS version 1c (Woodruff 2001a,b) was used in this study to produce maps of vector-wind regression coefficients upon an ENSO index, and time series of SST, SLP, and winds for selected regions. This new version of COADS incorporates additional observations for the years prior to 1950. We have observed that relationships derived from this data set for these years tend to be slightly stronger than those obtained with earlier versions of COADS. For the vector wind regressions, the anomaly fields were smoothed with successive 7- and 5-point running means along latitude circles, in which each grid point is weighted by the number of observations. The

running means take the average of all available data, and as such act to fill small patches of 2° latitude-longitude boxes for which there are no values. The percentage of COADS ocean grid boxes with data in a given month varies from 10% in the 1850s to 55% in the 1980s and 1990s; use of the running mean smoother typically fills an additional 10–30% of the ocean grid boxes. The effective resolution of the smoothed and interpolated data is 28 degrees of longitude and 4 degrees of latitude. This processing methodology is the same as was used by Mitchell and Wallace (1996) to compare ENSO variability in the 1950-78 and 1979-92 epochs.

3. ENSO indices

a. The cold tongue SST anomaly index (*CTI*)

The annual mean SST climatology for the tropical Pacific (Figure 1) features a prominent “cold tongue” extending from Ecuador to near the dateline. The cold tongue and the coastal regions of Peru and Ecuador experience large, ENSO-related month-to-month SST variations (indicated by the shading in Fig. 1), characterized by longitudinally coherent fluctuations extending across the eastern and central Pacific. It is well represented by the SST anomaly averaged over all the 2° latitude-longitude grid boxes within the dashed rectangular region in the figure (6°N–6°S, 90°–180° W). Our “cold tongue index” (CTI) is formed by taking this average each month and subtracting from it the global mean SST anomaly for the same month. Prior to 1998, the CTI time series in this paper is based on the COADS, in which each grid box is weighted by the number of observations for that year / month. Decade by decade sampling rates are listed in the second column of Table 2. From 1998 onward (through 2000) the CTI is based on the National Centers for Environmental Prediction (NCEP) analyses derived from the leading EOFs of the SST field (Smith et al. 1996). (Indices based on the COADS and NCEP data sets are correlated at a level of 0.95 for the common period of record 1950-97.)

Subtracting out the global-mean SST anomaly, as in Zhang et al. (1997), has the effect of defining the status of ENSO in terms of the shape of the SST pattern, rather than in terms of SST

level within the cold tongue region. Since the year-to-year variations in SST within the cold tongue region are a factor of ~ 5 larger than the corresponding variations in global-mean SST, this adjustment has a negligible effect upon the appearance of the CTI time series on the year-to-year time scale. However, it virtually eliminates the influence of the secular trend toward higher SST that has occurred in association with global warming. It should also reduce the influence of an abrupt increase of almost $0.5\text{ }^{\circ}\text{C}$ in COADS SSTs around 1942 due to changes in the measurement practices (Barnett 1984; Folland and Parker 1995). The CTI time series is not standardized, it does not have a mean value of zero (owing to the fact that the reference period 1950-79 was relatively cold), and it is not smoothed beyond monthly averages in the time domain.

An extended time series of the CTI for the period 1854-2000 is shown in Figure 2. Included for comparison are values of the CTI based on the LDEO SST field. Much of the difference in the appearance of the two time series during the earlier years of the record is attributable to the temporal smoothing inherent in the LDEO objective analysis scheme. From ~ 1870 onward, the two series track one another quite closely and the unsmoothed COADS-based time series exhibits a remarkable amount of month-to-month persistence. Digital values of the COADS / NCEP CTI are at provided as an electronic supplement at <http://jisao.washington.edu/data/mw02/> (the URL to be furnished by the AMS).

b. The east Indian pressure anomaly index (*EIPI*)

Pressure records beginning as early as the 1840s for land stations bordering the eastern Indian Ocean are combined to produce an index of ENSO variability. The stations included in the index, chosen on the basis of the strength of their SLP correlations with the CTI (Figure 3), are Trivandrum (now called Thiruvananthapuram) (8°N , 76°E) near the southern tip of India, Port Blair (11°N , 92°E) in the Andaman Islands in the Bay of Bengal, Djakarta Indonesia (formerly called Batavia) (6°S , 106°E), and Darwin Australia (12°S , 131°E). The records for Trivandrum and Port Blair were obtained from the National Center for Atmospheric Research (NCAR) World

Monthly Surface Station Climatology, Djakarta from Können et al. (1998) and Können (personal communication 2000), and Darwin from the University of East Anglia (UEA). Correlation coefficients between the SLP at each of these stations and the CTI during three successive ~50-year epochs (Table 3) are consistently strong and positive. The surface pressure anomalies, smoothed with a 3-month running mean, were averaged together using weights derived from principal component (PC) analysis of these four records based on the years 1900-95 (weights: Trivandrum 0.81, Port Blair 0.90, Djakarta 0.94, and Darwin 0.86), and a 3-month running mean was applied again. This index, henceforth referred to as the east Indian pressure index (EIPI), is plotted in Figure 4 along with Berlage's (1966) index of 6-month average pressures from around the Indian Ocean, and the 3-month average multivariate (SLP, temperature, and precipitation) Southern Oscillation (SO) indices of Walker and Bliss (1932, 1937). The EIPI, Berlage, and Walker and Bliss indices are standardized with respect to the period of common record, 1882-1929. Both the EIPI and Berlage indices are measures of SLP in the Darwin pole of the SO, while the Walker and Bliss index is based on SO-related variables from around the globe. The Berlage index includes Djakarta and Darwin, in common with the EIPI; Bombay and Madras for the entire record; and Capetown, Mauritius, Perth, Adelaide, and Hobart for shorter intervals.

The Berlage series represents anomalies relative to consecutive 30-year means, and is consequently suitable only for documenting year-to-year variability. Changes in the station location or measurement practices for Trivandrum and Port Blair during the decades of the 1950s-1970s required the use of multiple climatologies, and so decadal and longer term changes in the EIPI are probably underrepresented after 1950. The EIPI, Berlage, and Walker and Bliss indices in Fig. 4 portray a mutually consistent picture of the year-to-year variability throughout their common record. Digital values of the EIPI are available at <http://jisao.washington.edu/data/mw02/> (the URL to be provided by the AMS).

c. The dynamical ENSO index (*DEI*)

A third ENSO index was constructed by combining indices of tropical rainfall, SLP, and surface wind anomalies, variables which fluctuate in synchrony during the ENSO cycle. The averaging regions for the indices were determined by correlating monthly anomalies of each variable with the CTI for 1950-79, as was performed with eastern Indian Ocean SLP in the EIPI calculation. Simplified correlation maps indicating the averaging regions are shown in Figure 5. Data sources and sampling statistics for each variable and region are listed in Tables 1 and 2, respectively.

- The SO in tropical marine SLP anomalies is represented in terms of two indices: D* the average for grid boxes in which SLP is positively correlated with the CTI (shaded region in Fig. 5a), and T* the average for grid boxes in which SLP is negatively correlated with the CTI (the unshaded region between 20°N-20°S in Fig. 5a). The labels D* and T* match the Darwin Australia and Tahiti poles of the conventional SO, respectively. The contribution of individual grid boxes to each index is weighted by its SLP-CTI correlation coefficient and the number of observations in each year / month. These indices are also combined to produce a SO index based on marine observations: $SOI^* = \text{standardized}(T^*) - \text{standardized}(D^*)$, with the standardization performed separately for each calendar month based on statistics for the years 1950-79.

- ENSO-related variability in the wind field is represented by average zonal wind anomalies averaged over the western equatorial Pacific (8°N-8°S, 150°E-140°W), denoted as U in Fig. 5b, and meridional wind anomalies averaged over the region to the north of the equator (2-12°N, 160°E-70°W), denoted as V in Fig. 5b. The contribution of individual grid boxes to each index is weighted by the number of observations in each year / month.

- The indices "PR" (Pacific rainfall) and "nPR" (non-Pacific rainfall) are measures of the rainfall in regions strongly influenced by ENSO. PR represents an average over the equatorial Pacific (6.25°N-6.25°S, 163.75°E-86.25°W; heavily shaded in Fig. 5c), where rainfall tends to be

enhanced during warm episodes of the ENSO cycle, and "nPR" an average over 20°N-20°S, 78.75°W-163.75°E (lightly shaded in Fig. 5c), where rainfall tends to be suppressed.

Regional time series similar to those defined above have been used in earlier studies by Wyrski (1975), Meisner (1976), Barnett (1977), Wright (1977, 1979), Reiter (1978), Angell (1981), Rasmusson and Carpenter (1982), Wright et al. (1988), Zhang et al. (1997), and others. The present study builds on these earlier works by analyzing longer records and, in the following, by combining the series.

PC analysis was applied to D*, T*, U, V, PR, and nPR to identify the common variations in these series. The relative contribution of each series to the PC is determined from monthly values of the series for 1920-95, smoothed with a 3-month running mean (weights: D* 0.73, T* 0.73, U 0.72, V 0.76, PR 0.78, and nPR 0.79). An extended 1870-1997 time series is obtained by projecting monthly data, smoothed with 3-month running mean, onto the loading vector of the PC. The extended time series, smoothed with an additional pass of a 3-month running mean, is hereafter referred to as the dynamical ENSO index (DEI). Fluctuations in this index explain 50% of the combined variance of D*, T*, U, V, PR, and nPR over the historical record 1870-1997.

The DEI, the six constituent series, and the SOI* are plotted in Figure 6. The agreement between the PC and its constituent series is very good from 1875 to the present. [Unfiltered monthly digital values of the indices in Fig. 6 are given at <http://jisao.washington.edu/data/mw02/> --- the URL to be provided by the AMS.]

4. Comparison of time series

The CTI, DEI, and EIPI are independent representations of ENSO variability, extending back to the mid-1800s, that augment the Darwin, Djakarta, and Tahiti station records from which much of our understanding of historical ENSO variability is derived. In this section, the relationships between the CTI, EIPI, and DEI are quantified, and filtered versions of these series are presented

to document ENSO variability on seasonal, year-to-year, and decadal time scales. For all of the graphical presentations the time series are standardized with respect to the common period of record of the series, 1870-1997.

Figure 7 shows the CTI, DEI, and EIPI as monthly time series. The DEI and EIPI are smoothed by construction, and the CTI is smoothed with a 3-month running mean in this figure to make it consistent with them. The time series are plotted in ~50 year segments so that the consistency between the indices in individual years can be assessed. The qualitative agreement between the series is very good back to the 1870s, as evidenced by correlations in excess of 0.70 between all pairs of the series for the common record, 1870-1997.

Figure 8 displays the CTI, EIPI, and DEI plotted as annualized indices (one value per year), in which it is easier to assess the strength of individual warm and cold events and the recurrent interval of strong events. The indices in Fig. 8 are averages of the input monthly series from July of one year to February of the next year, with the value ascribed to the year of the July. This choice of calendar months for the averaging period is dictated by the observed persistence of ENSO anomalies in these months. Digital values of the indices are provided in Table 4 and at <http://jisao.washington.edu/data/mw02/> (the URL to be furnished by the AMS). The correlations between each pair of series is in excess of 0.84 for 1870-1997.

In recent decades ENSO variability in the tropical Pacific has exhibited a distinct seasonality, with anomalies of one sign in April-July tending to persist into the early months of the following year (Walker and Bliss 1932; Troup 1965; Wright 1977, 1979, 1985; Trenberth and Shea 1987; Wallace and Jiang 1988; Webster and Yang 1992; Torrence and Webster 1998). Figure 9 shows autocorrelation statistics for the CTI and DEI, stratified by calendar month for each of the three ~50 year epochs. Each row of the analysis is the autocorrelation of the given variable in a calendar month with each of the subsequent 12 months. The tendency for a diminished autocorrelation of both the DEI and CTI in February-March-April is evident in all three epochs.

Decadal and longer-time scale ENSO variability in the CTI, DEI, and EIPi are shown in Figure 10, in which the individual time series are smoothed by application of successive 5- and 3-year running means. The series show a general agreement from the mid-1890s to 1995, with generally warm ENSO conditions during 1900-1915, cool during 1945-60, and warm during the 1980s and 1990s. The warm bias of the ENSO cycle during the early 1900s was comparable to the warm bias since the late 1970s. Although these indices exhibit many of the same features, they are generally less consistent with one another with regard to their representation of the decadal scale variability than the year-to-year variability associated with the ENSO cycle.

5. Spatial structure

In this section, we make use of the extended time series of the CTI together with various extended data sets for atmospheric fields to assess the extent to which the spatial signature of ENSO as determined from data from 1950 onward is representative of the observed structure in prior segments of the record.

Figures 11 and 12 show fields of monthly SST, land SAT, surface vector wind, SLP, and land precipitation anomalies regressed onto the standardized CTI for three successive segments of the record. All calendar months are included in this analysis. The SST and SLP analyses in Figs. 11 and 12 complement correlation maps presented for 20-year epochs and stratified by season in Allan et al. (1996), and the land SAT and precipitation analyses complement the composite studies of Kiladis and Diaz (1989), Ropelewski and Halpert (1986, 1987, 1989), Halpert and Ropelewski (1992), and others. The regression coefficients shown on the maps may be interpreted as typical anomalies in a given field for a typical ENSO episode in each epoch (defined by 1 standard deviation of the CTI). The signature of ENSO in the anomaly fields over the tropical Pacific and eastern Indian Ocean is evident in all 3 epochs.

Most of the familiar features over tropics and the Americas in the bottom panels Figs. 11 and 12 that have been identified in analyses based on data from 1950 onward are recognizable in the

earlier segments of the record, to the extent that data are available to reveal them. An exception is the negative temperature anomalies over the southeastern United States, first noted by Ropelewski and Halpert (1986), which are reproducible in data for the first half of the 20th century but not in the 19th century segment of the record.

Further documentation of the patterns of surface air temperature over land areas of the extratropical Northern Hemisphere is provided in the form of polar stereographic maps shown in Figure 13. Panels (a) and (b) are based on a recently released analysis of SAT from the UEA (New et al. 2000) and (c) on the NCEP / NCAR Reanalysis (Kistler et al. 2001). As noted above, the features over North America are reproducible during the two halves of the 20th century, and the same is true of most of the features over Asia. All the features in the SAT field in the second half of the 20th century are mirrored in the lower tropospheric thickness field (panel (c)). The most notable discrepancies between the patterns for the first and second halves of the 20th century are over Europe and the Middle East. During the second half of the century Northern Europe experienced near normal to slightly above normal temperatures during El Niño years, whereas during the first half of the century temperatures tended to be below normal. It is evident from Fig. 11 that Northern Europe tended to be cold during El Niño years of the late 19th century as well. Evidently, the El Niño signal is less robust over this portion of the hemisphere than elsewhere, perhaps because it lies at the downstream end of a long wavetrain originating in the Pacific sector.

6. Discussion

The results presented in this paper are largely qualitative and descriptive. Warm and cold episodes of the ENSO cycle have been defined, not in terms of deviations from a time varying climatology that takes into account the warming trend in the SST record, but on the basis of the SST pattern in the equatorial Pacific cold tongue region, and ancillary indices based solely on atmospheric data.

The data from 1870 onward appear to be adequate for defining the more prominent swings in the ENSO cycle, as evidenced by the consistency of the three indices plotted in Figs. 7, 8, and 10. One notable exception is a brief period in 1917, when the SST observations in the equatorial Pacific are indicative of neutral ENSO cycle conditions, while the pressure, rainfall, and wind data are all indicative of a rather strong cold episode. Very few SST observations were available at that time, which coincides with World War I.

Each of the 50 year epochs considered in this study witnessed at least one warm episode of the ENSO cycle that may well have been comparable in magnitude to the 1982-83 and 1997-98 El Niño events. Both of the segments of Fig. 8 contains on the order of 10 well defined warm episodes (as reflected in all three indices), interspersed with colder intervals. The 1991-95 warm episode was unusual in terms of its duration, but it is rivaled by the 1911-14 and 1939-41 episodes. Extended cold episodes occurred in the 1916-18 and 1954-57, and the decades of the 1870's and 1930's were characterized by the prevalence of cold polarity of ENSO. Positive values of the CTI have been prevalent since 1977, but there were analogous warm intervals earlier in the record (e.g., 1895-1931). Hence, neither the CTI, the DEI, nor the EIPI offers striking visual evidence of secular trends in the characteristics of the ENSO cycle. To test this impression, the reader is invited to select from the five rearranged segments of the CTI time series shown in Figure 14 (some of which have been inverted in time), the one that corresponds to the most recent 25 year segment of the record. (The original CTI series is presented in Figure 15 as an answer key.) It is equally difficult to distinguish secular changes in the ENSO cycle behavior in the DEI and EIPI (not shown).

The indices appear to be less consistent with respect to the depiction of the interdecadal-scale ENSO-related variability than the year-to-year swings of the ENSO cycle. Figure 10 reflects the shift toward the warm polarity around 1976-77 that has been noted by Nitta and Yamada (1989) Trenberth (1990), Graham (1994), and others, and the shift in the opposite direction in the mid-1940s noted by Zhang et al. (1997), but it does not show this "regime like" behavior as clearly and

consistently as studies based on the leading empirical orthogonal function of the global SST field (Zhang et al. 1997) or selected North Pacific and Indian Ocean time series (Mantua et al. 1997; Minobe 1997, 1999).

Acknowledgements

This research was supported by the National Oceanic and Atmospheric Administration Office of Global Programs and the Earth Resources Laboratory through a grant to the Stanley P. Hayes Center for the Study of Climate Variability at the University of Washington. We thank Tracy Basnett of the United Kingdom Meteorological Office (UKMO) for comparing the SLP analysis in Fig. 12 with historical UKMO SLP data, and Alexey Kaplan of LDEO for providing updated SLP analyses (not shown) for Fig. 12. David Parker provided helpful comments on the manuscript. This publication is (partially) funded by the Joint Institute for the Study of the Atmosphere and Ocean (JISAO) under NOAA Cooperative Agreement No. NA17RJ1232. JISAO contribution number 869.

REFERENCES

- Allan, R. J., and R. D. D'Arrigo, 1999: "Persistent" ENSO sequences: How unusual was the 1990-1995 El Niño? *The Holocene*, **9**, 101-118.
- _____, J. Lindesay, and D. Parker, 1996: *El Niño Southern Oscillation and Climatic Variability*. Commonwealth Scientific and Industrial Research Organisation (CSIRO), 405 pp.
- Angell, J. K., 1981: Comparison of variations in atmospheric quantities with sea surface temperature variations in the equatorial eastern Pacific. *Mon. Wea. Rev.*, **109**, 230-243.
- Barnett, T. P., 1977: The principal time and space scales of the Pacific trade wind fields. *J. Atmos. Sci.*, **34**, 221-236.
- _____, 1984: Long-term trends in surface temperature over the oceans. *Mon. Wea. Rev.*, **112**, 303-312.
- Basnett, T. A., and D. E. Parker, 1997: Development of the global mean sea level pressure data set GMSLP2. Tech. Rep. CRTN 79, Hadley Centre for Climate Prediction and Research, 51 pp. [Available from Meteorological Office, London Road, Bracknell, Berkshire RG12 2SY, United Kingdom.]
- Berlage, H. P., 1966: *The Southern Oscillation and world weather*. K. Ned. Meteor. Inst. Meded. Verh., **88**, 153 pp.

- Dai, A., I. Y. Fung, and A. Del Genio, 1997: Surface observed global land precipitation variations during 1900-88. *J. Climate*, **10**, 2943-2962.
- Fedorov, A. V., and S. G. H. Philander, 2000: Is El Niño changing? *Science*, **288**, 1997-2002.
- Folland, C. K., and D. E. Parker, 1995: Correction of instrumental biases in historical sea surface temperature data. *Quart. J. Roy. Meteor. Soc.*, **121**, 319-367.
- Graham, N. E., 1994: Decadal-scale climate variability in the 1970s and 1980s: Observations and model results. *Climate Dyn.*, **10**, 135-162.
- Halpert, M. S., and C. F. Ropelewski, 1992: Surface temperature patterns associated with the Southern Oscillation. *J. Climate*, **5**, 577-593.
- Harrison, D. E., and N. K. Larkin, 1997: Darwin sea level pressure, 1876-1996: Evidence for climate change? *Geophys. Res. Lett.*, **24**, 1779-1782.
- Jones, P. D., T. J. Osborn, K. R. Briffa, C. K. Folland, E. B. Horton, L. V. Alexander, D. E. Parker, and N. A. Rayner, 2001: Adjusting for sampling density in grid box land and ocean surface temperature time series. *J. Geophys. Res.*, **106**, 3371-3380.
- Kaplan, A., Y. Kushnir, M. A. Cane, and M. B. Blumenthal, 1997: Reduced space optimal analysis for historical data sets: 136 years of Atlantic sea surface temperatures. *J. Geophys. Res.*, **102**, 27835-27860.

- Kaplan, A., M. A. Cane, Y. Kushnir, A. C. Clement, M. B. Blumenthal, and B. Rajagopalan, 1998: Analyses of global sea surface temperature 1856-1991. *J. Geophys. Res.*, **103**, 18567-18589.
- _____, Y. Kushnir, and M. A. Cane, 2000: Reduced space optimal interpolation of historical marine sea level pressure: 1854-1992. *J. Climate*, **13**, 2987-3002.
- Kiladis, G. N., and H. F. Diaz, 1989: Global climatic anomalies associated with extremes in the Southern Oscillation. *J. Climate*, **2**, 1069-1090.
- Kistler, R., E. Kalnay, W. Collins, S. Saha, G. White, J. Woollen, M. Chelliah, W. Ebisuzaki, M. Kanamitsu, V. Kousky, H. van den Dool, R. Jenne, and M. Fiorino, 2001: The NCEP-NCAR 50-year reanalysis: Monthly means CD-ROM and documentation. *Bull. Amer. Meteor. Soc.*, **82**, 247-268.
- Können, G. P., P. D. Jones, M. H. Kalkofen, and R. J. Allan, 1998: Pre-1866 extensions of the Southern Oscillation Index using early Indonesian and Tahitian meteorological readings. *J. Climate*, **11**, 2325-2339.
- Mantua, N. J., S. R. Hare, Y. Zhang, J. M. Wallace, and R. C. Francis, 1997: A Pacific interdecadal climate oscillation with impacts on salmon production. *Bull. Amer. Meteor. Soc.*, **78**, 1069-1079.
- Meisner, B. N., 1976: A study of Hawaii and Line Island rainfall. Rep. UHMET-74-04, Dept. Meteor., Univ. Hawaii, 83 pp.

Minobe, S., 1997: A 50-70 year climatic oscillation over the north Pacific and North America. *Geophys. Res. Lett.*, **24**, 683-686.

_____, 1999: Resonance in bidecadal and pentadecadal climate oscillations over the north Pacific: Role in climatic regime shifts. *Geophys. Res. Lett.*, **26**, 855-858.

Mitchell, T. P., and J. M. Wallace, 1996: ENSO seasonality: 1950-78 versus 1979-92. *J. Climate*, **9**, 3149-3161.

Nitta, T., and S. Yamada, 1989: Recent warming of tropical sea surface temperature and its relationship to the Northern Hemisphere circulation. *J. Meteor. Soc. Japan*, **67**, 375-383.

New, M., M. Hulme, and P. Jones, 2000: Representing twentieth-century space-time climate variability. Part II: Development of 1901-96 monthly grids of terrestrial surface climate. *J. Climate*, **13**, 2217-2238.

Rajagopalan, B., U. Lall, and M. A. Cane, 1997: Anomalous ENSO occurrences: An alternative view. *J. Climate*, **10**, 2351-2357.

_____, _____, and _____, 1999: Comment on "Reply to the comments of Trenberth and Hurrell." *Bull. Amer. Meteor. Soc.*, **80**, 2724-2726.

Rasmusson, E. M., and T. H. Carpenter, 1982: Variations in tropical sea surface temperature and surface wind fields associated with the Southern Oscillation / El Niño. *Mon. Wea. Rev.*, **110**, 354-384.

Reiter, E. R., 1978: Long-term wind variability in the tropical Pacific, its possible causes and effects. *Mon. Wea. Rev.*, **106**, 324-330.

Ropelewski, C. F., and M. S. Halpert, 1986: North American precipitation and temperature patterns associated with the El Niño / Southern Oscillation (ENSO). *Mon. Wea. Rev.*, **114**, 2352-2362.

_____, and _____, 1987: Global and regional scale precipitation patterns associated with the El Niño / Southern Oscillation. *Mon. Wea. Rev.*, **115**, 1606–1626.

_____, and _____, 1989: Precipitation patterns associated with the high index phase of the Southern Oscillation. *J. Climate*, **2**, 268-284.

Smith, T. M., R. W. Reynolds, R. E. Livezey, and D. C. Stokes, 1996: Reconstruction of historical sea surface temperatures using empirical orthogonal functions. *J. Climate*, **9**, 1403-1420.

Stahle, D. W., R. D. D'Arrigo, P. J. Krusic, M. K. Cleaveland, E. R. Cook, R. J. Allan, J. E. Cole, R. B. Dunbar, M. D. Therrell, D. A. Gay, M. D. Moore, M. A. Stokes, B. T. Burns, J. Villanueva-Diaz, and L. G. Thompson, 1998: Experimental dendroclimatic reconstruction of the Southern Oscillation. *Bull. Amer. Meteor. Soc.*, **10**, 2137-2152.

Torrence, C., and P. J. Webster, 1998: The annual cycle of persistence in the El Niño / Southern Oscillation. *Quart. J. Roy. Meteor. Soc.*, **124**, 1985-2004.

- Trenberth, K. E, 1990: Recent observed interdecadal climate changes in the Northern Hemisphere. *Bull. Amer. Meteor. Soc.*, **71**, 988-993.
- _____, and D. Shea, 1987: On the evolution of the Southern Oscillation. *Mon. Wea. Rev.*, **115**, 3078-3096.
- _____, and T. J. Hoar, 1996: The 1990-1995 El Niño - Southern Oscillation event: Longest on record. *Geophys. Res. Lett.*, **23**, 57-60.
- _____, and J. W. Hurrell, 1999a: Comments on "The interpretation of short climate records with comments on the North Atlantic and Southern Oscillations." *Bull. Amer. Meteor. Soc.*, **80**, 2721-2722.
- _____, and _____, 1999b: Reply to Rajagopalan, Lall, and Cane's comment about "The interpretation of short climate records with comments on the North Atlantic and Southern Oscillations." *Bull. Amer. Meteor. Soc.*, **80**, 2726-2728.
- _____, and D. P. Stepaniak, 2001: Indices of El Niño evolution. *J. Climate*, **14**, 1697-1701.
- Troup, A. J., 1965: The Southern Oscillation. *Quart. J. Roy. Meteor. Soc.*, **91**, 490-506.
- Urban, F. E., J. E. Cole, and J. T. Overpeck, 2000: Influence of mean climate change on climate variability from a 155-year tropical Pacific coral record. *Nature*, **407**, 989-993.
- Walker, G., T., and E. W. Bliss, 1932: World weather V. *Mem. Roy. Meteor. Soc.*, **4**, No. 36, 53-84.

Walker, G. T., and E. W. Bliss, 1937: World weather VI. *Mem. Roy. Meteor. Soc.*, **4**, No. 39, 119-139.

Wallace, J. M., and Q. Jiang, 1988: On the observed structure of the interannual variability of the atmosphere / ocean climate system. *Atmospheric and Oceanic Variability*, H. Cattle, Ed., Roy. Meteor. Soc., 17-43.

Webster, P. J., and S. Yang, 1992: Monsoon and ENSO: Selectively interactive systems. *Quart. J. Roy. Meteor. Soc.*, **118**, 877-926.

Woodruff, S. D., 2001a: COADS updates including newly digitized data and the blend with the United Kingdom Meteorological Office Marine Data Bank. *Workshop on Prep., Process., and Use of Hist. Marine Meteor. Data*. Tokyo, Japan Meteor. Agency and Ship and Ocean Found., 9-13. [http://www.cdc.noaa.gov/coads/jma00_a.html]

_____, 2001b: Quality control in recent COADS updates. *Workshop on Prep., Process., and Use of Hist. Marine Meteor. Data*. Tokyo, Japan Meteor. Agency and Ship and Ocean Found., 49-53. [http://www.cdc.noaa.gov/coads/jma00_b.html]

Wright, P. B., 1977: The Southern Oscillation – patterns and mechanisms of the teleconnections and the persistence. Rep. HIG-77-13, Hawaii Inst. Geophys., University of Hawaii, Honolulu HI, 107 pp.

_____, 1979: Persistence of rainfall anomalies in the central Pacific. *Nature*, **277**, 371-374.

Wright, P. B., 1985: The Southern Oscillation: An ocean-atmosphere feedback system? *Bull. Amer. Meteor. Soc.*, **66**, 398-412.

_____, J. M. Wallace, T. P. Mitchell, and C. Deser, 1988: Correlation structure of the El Niño / Southern Oscillation phenomenon. *J. Climate*, **1**, 609-625.

Wunsch, C., 1999a: The interpretation of short climate records with comments on the North Atlantic and Southern Oscillations. *Bull. Amer. Meteor. Soc.*, **80**, 245-256.

_____, 1999b: Reply to comments on "The interpretation of short climate records with comments on the North Atlantic and Southern Oscillations." *Bull. Amer. Meteor. Soc.*, **80**, 2723.

Wyrtki, K., 1975: El Niño – the dynamic response of the equatorial Pacific Ocean to atmospheric forcing. *J. Phys. Oceanogr.*, **5**, 572-584.

Zhang, Y., J. M. Wallace, and D. S. Battisti, 1997: ENSO-like interdecadal variability: 1900-93. *J. Climate*, **10**, 1004-1020.

Figure Captions

FIG. 1. Annual-mean SST (contours) and standard deviation of monthly mean SST anomalies (shading) for 1950-79. Contour interval 1°C , with the 27°C isotherm thickened, and “W”s denote the warmest SSTs. Shading for standard deviations $> 1^{\circ}\text{C}$. The dashed rectangle defines the area average for the cold tongue index.

FIG. 2. CTI for 1854-99, 1900-49, and 1950-2000 from the COADS / NCEP and LDEO SST data sets. The anomalies are with respect to 1950-79, and the intervals between tick marks on the ordinate and abscissa tick are 1°C and 1 year, respectively.

FIG. 3. Map of correlation coefficients between COADS SLP anomalies and the CTI for 1950-79. Light (dark) shading over the oceans denotes correlation > 0 (> 0.5), and the four stations used for the EIPI are labeled. Both variables are smoothed with a 3-month running mean.

FIG. 4. The EIPI, Berlage (“B”), and Walker and Bliss (“WB”) time series plotted in segments for 1841-49, 1850-99, 1900-49, and 1950-2000. All series are standardized with respect to the period of common record, 1882-1929. Ordinate and abscissa tick intervals are 2 standard deviations and 1 year, respectively.

FIG. 5. Averaging regions for a) D^* and T^* SLP anomaly indices, b) U and V zonal and meridional surface wind anomaly indices, and c) PR and nPR rainfall indices. See text for definitions. In a) marine SLP-CTI correlations are plotted for 20°N - 20°S , with no, light, and dark shading over the oceans for correlations < 0 , 0 - 0.5 , > 0.5 ; and a dashed contour for correlations of -0.5 . In c) the PR and nPR indices are the average, within 20°N - 20°S , of precipitation anomalies in the dark and light shaded land regions, respectively.

FIG. 6. DEI, U, V, PR, D*, T*, SOI*, and nPR indices plotted for a) 1870-1939 and b) 1930-97. The monthly time series have been smoothed with successive 13- and 7-month running means, and the time series are standardized in each panel. The V, T*, SOI*, and nPR indices are inverted such that positive values are associated with an ENSO warm episode. Gray and black shading indicates months in which the time series value is of the same and opposite polarity to that of the DEI, respectively, and the correlation coefficient *100 of each series with the DEI is indicated on the right border. Ordinate tick interval of 2 standard deviations.

FIG. 7. Monthly values of the CTI, DEI, and EIPI, plotted for 1841-49, 1850-99, 1900-49, and 1930-2000. The CTI is smoothed with a 3-month running mean, and all of the time series are standardized with respect to 1870-1997. Ordinate and abscissa tick intervals of 2 standard deviation and 1 year, respectively.

Fig. 8. As in Fig. 7, but for annualized values of the CTI, DEI, and EIPI, with the annual values defined as the average from July of one year to February of the next. The annualized values are ascribed to the year of the July.

FIG. 9. Lag-correlation statistics, stratified by calendar month, for the DEI and CTI for successive ~50 year epochs. Each row of a panel is the lag-correlations for the time series beginning in a given calendar month with each of the successive 12 months, and the 12 rows are repeated. Light, darker, and darkest shading indicates correlation magnitudes of 0.3, 0.6, and 0.9, respectively. The DEI record spans 1870-1997.

Fig. 10. As in Fig. 7, but for monthly values of the CTI, DEI, and EIPI smoothed with successive 5- and 3-year running means. The first and last 2.5 years of each filtered time series is removed to eliminate the undue influence of end points. The ordinate tick interval is 1 standard deviation.

FIG. 11. Monthly SST, land SAT, and marine surface vector wind anomalies regressed upon normalized values of the CTI for a) 1854-99, b) 1900-49, and c) 1950-2000. The regression coefficients are scaled to indicate the typical anomalies in each field that correspond to a one standard deviation positive anomaly in the CTI for that epoch. SST contour interval of 0.25 °C per standard deviation of the CTI: the zero line is thickened and negative contours are dashed. Land temperatures in units of °C per standard deviation of the CTI. Only vector winds with magnitudes $> 0.5 \text{ m s}^{-1}$ per standard deviation of the CTI and at least 100 months of observations in an epoch are plotted. Data sources are given in Table 1.

FIG. 12. As in Fig. 11, but for monthly marine SLP, land rainfall, and vector surface wind anomalies regressed upon normalized values of the CTI for a) 1854-99, b) 1900-49, and c) 1950-97. SLP contour interval of 0.25 hPa per standard deviation of the CTI: the zero line is thickened and negative contours are dashed. Rainfall units of cm/mon per standard deviation of the CTI, and rainfall is plotted with a nonlinear scale to capture the smaller magnitude anomalies in the extratropics. The vector wind regressions are repeated from Fig. 11.

FIG. 13. As in Fig. 11, but for UEA land SAT anomalies for a) 1901-49 and b) 1950-95, and c) NCEP / NCAR reanalysis SAT (shading) and 1000-500 hPa thickness (contours) for 1950-95. Thickness contour interval of 4m per standard deviation of the CTI with negative, zero, and positive isopleths plotted as dashed, thick solid, and thin solid contours, respectively. The 0.5° latitude-longitude resolution UEA data have been averaged into 1° latitude-longitude grid boxes. The reanalysis data have 2.5° latitude-longitude resolution.

FIG. 14. Synthetic monthly ENSO temperature time series (°C), derived from the CTI for 1876-2000. The synthetic series is constructed by reversing time for the CTI, breaking the series up into 25-year segments, and reordering the segments. The time series is smoothed with a 3-month running mean. The ordinate and abscissa tick intervals are 1° C and 1 year, respectively, and a light vertical line is plotted for every 5th year .

FIG. 15. As in Fig. 14, but for the actual monthly CTI time series (°C).

Tables

Table 1. Gridded data sets employed in the study, the period of record used for each analysis, and references. Abbreviations are defined at the bottom of the table.

	<u>variable</u>	<u>years</u>	<u>reference</u>
Fig. 1	SST	1950-79	COADS (Woodruff 2001a,b)
Fig. 2	SST	1854–1997	COADS
	SST	1998-2000	NCEP (Smith et al. 1996)
	SST	1856–2000	LDEO (Kaplan et al. 1997, 1998)
Fig. 3	SLP	1950-79	COADS
Fig. 5	SLP, vector wind	1950-79	COADS
	rainfall	1950-79	NASA (Dai et al. 1997)
Fig. 6	SLP, vector wind	1854-1997	COADS
	rainfall	1854-1996	NASA
Fig. 11	SST	1856–2000	LDEO
	land SAT	1854–2000	UEA (Jones et al. 2001)
	vector wind	1854–1997	COADS
Fig. 12	SLP	1854–1992	LDEO (Kaplan et al. 2000)
	rainfall	1854–1996	NASA
	vector wind	1854–1997	COADS
Fig. 13	SAT	1901-95	UEA (New et al. 2000)
	SAT	1950-95	NCEP / NCAR (Kistler et al. 2001)
	1000-500 hPa thickness	1950-95	NCEP / NCAR

Abbreviations:

surface air temperature	SAT
Comprehensive Ocean-Atmosphere Data Set	COADS
Lamont-Doherty Earth Observatory	LDEO
National Aeronautics and Space Agency	NASA
National Centers for Environmental Prediction	NCEP
National Center for Atmospheric Research	NCAR
University of East Anglia	UEA

Table 2. Average number of observations or grid boxes contributing per month for the CTI and the DEI input series. The statistics are aggregated by decade to simplify the presentation. Number of observations information is not available for the rainfall data set, and the sampling rates for PR and nPR are given as the number of grid boxes with data. Statistics for the period around World War I in italics.

Decade	CTI (obs.)	U (obs.)	V (obs.)	PR (boxes)	D* (obs.)	T* (obs.)	nPR (boxes)
1850-59	42	24	79	0	908	90	45
1860-69	6	8	15	0	1265	17	61
1870-79	38	18	48	0	1130	34	109
1880-89	92	52	128	0	2053	120	162
1890-99	95	30	139	4	3156	155	255
1900-09	87	56	159	8	4226	277	396
1910-19	77	61	219	10	5840	686	479
<i>1914-1920</i>	<i>33</i>	<i>51</i>	<i>190</i>	<i>9</i>	<i>4786</i>	<i>721</i>	<i>488</i>
1920-29	128	106	518	11	10076	2089	589
1930-39	169	230	683	18	12398	3197	690
1940-49	138	277	626	17	5169	1961	680
1950-59	313	203	1112	30	13320	5534	841
1960-69	659	606	2026	30	26400	9026	864
1970-79	912	847	2204	27	29620	9807	815
1980-89	1612	1531	2513	14	32448	9240	701
1990-97	16801	12264	12139	5	26437	7764	511

Table 3. Correlation coefficients *100 of the CTI with monthly surface pressure anomalies for selected stations, stratified for three ~50 year epochs. The period of record and percentage of complete records for each station are also provided. All time series are smoothed with a 3-month running mean for the correlation calculation. The CTI spans the years 1854-2000.

	Trivandrum	Port Blair	Djakarta	Darwin
correlation *100				
1854-99	39	69	56	61
1900-49	47	62	65	66
1950-2000	52	69	71	76
years	1853-2000	1871-2000	1841-1999	1866-2000
% complete record	84	86	94	100

Table 4. Digital values of the annualized CTI (°C), DEI (dimensionless), and EIPI (dimensionless)

* 100 for 1840-2000. The annualized values are July through February averages ascribed to the year of the July. Anomalies are with respect to 1870-1997, and the annualized DEI and EIPI are normalized with respect to 1870-1997. Standardized values of these indices are plotted in Fig. 8.

"," indicates no data.

	CTI	DEI	EIPI												
1840	.	.	.	1880	24	-72	122	1920	10	-17	-117	1960	-29	-28	-46
1841	.	.	7	1881	-15	-117	19	1921	-15	-13	-32	1961	-68	-63	-92
1842	.	.	-114	1882	-51	-82	-50	1922	-39	-40	-78	1962	-56	-62	-113
1843	.	.	-61	1883	.	-22	46	1923	67	84	44	1963	56	61	104
1844	.	.	-435	1884	62	50	92	1924	-69	-92	-83	1964	-53	-50	-98
1845	.	.	93	1885	42	-73	132	1925	84	113	116	1965	133	121	118
1846	.	.	34	1886	-100	-211	-156	1926	-23	-35	-114	1966	-33	-43	-32
1847	.	.	-81	1887	15	-44	72	1927	6	26	28	1967	-80	-34	16
1848	.	.	-259	1888	169	205	168	1928	-20	-2	-56	1968	46	9	21
1849	.	.	-230	1889	-79	-176	-150	1929	25	73	-6	1969	68	28	78
1850	.	.	-67	1890	-15	-38	22	1930	106	163	95	1970	-98	-104	-165
1851	.	.	2	1891	16	.	71	1931	-31	15	13	1971	-57	-48	-71
1852	.	.	102	1892	-112	-94	-37	1932	-5	-10	-65	1972	168	166	91
1853	-62	.	25	1893	-57	-139	-50	1933	-69	-113	-78	1973	-107	-148	-175
1854	-14	.	-42	1894	-28	-39	-9	1934	-24	-28	27	1974	-37	-59	-115
1855	58	.	123	1895	52	5	4	1935	10	7	3	1975	-93	-131	-151
1856	-71	.	-79	1896	148	113	123	1936	-25	14	-28	1976	102	83	21
1857	61	.	62	1897	-25	-49	-73	1937	-32	-27	-59	1977	24	57	96
1858	-26	.	63	1898	-56	-95	-96	1938	-69	-69	-95	1978	-23	1	-14
1859	-37	.	3	1899	99	136	145	1939	38	45	58	1979	28	49	57
1860	-85	.	-79	1900	37	49	24	1940	75	123	201	1980	-7	18	63
1861	-11	.	-121	1901	9	-23	61	1941	84	119	68	1981	-12	-19	-12
1862	-28	.	-274	1902	176	160	146	1942	-108	-68	-42	1982	178	217	215
1863	.	.	-82	1903	-33	-113	-70	1943	-46	.	44	1983	7	8	4
1864	157	.	210	1904	114	107	141	1944	-44	-57	-59	1984	-53	-23	-74
1865	-31	.	91	1905	130	106	93	1945	-40	-36	-8	1985	-39	-15	-17
1866	.	.	38	1906	-62	-43	-42	1946	-23	16	-31	1986	66	127	119
1867	-159	.	6	1907	47	15	6	1947	-35	-48	-14	1987	97	83	77
1868	180	.	91	1908	-76	-50	-44	1948	-46	23	-33	1988	-94	-118	-104
1869	-90	-146	-174	1909	-88	-80	-109	1949	-115	-82	-99	1989	-30	-11	38
1870	-74	-37	-135	1910	-47	-60	-108	1950	-95	-67	-116	1990	-4	31	77
1871	-8	-98	-92	1911	121	201	100	1951	68	43	16	1991	89	180	141
1872	-79	-129	-214	1912	7	50	-1	1952	-38	1	11	1992	4	115	59
1873	-64	-90	20	1913	62	113	167	1953	-1	20	14	1993	42	97	79
1874	-79	60	-100	1914	100	175	134	1954	-100	-86	-63	1994	46	112	128
1875	-62	-75	-80	1915	-16	-43	-76	1955	-143	-123	-157	1995	-71	-33	-38
1876	68	-81	100	1916	-85	-204	-189	1956	-65	-54	-59	1996	-38	-7	-53
1877	158	270	272	1917	-16	-124	-148	1957	105	114	95	1997	170	322	294
1878	-28	-225	-170	1918	149	186	158	1958	-11	42	4	1998	-93	.	-95
1879	-48	-187	-114	1919	29	75	45	1959	-22	-26	-49	1999	-117	.	-40
												2000	-63	.	-151

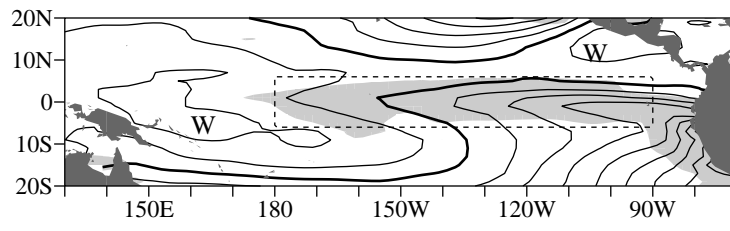


Figure 1

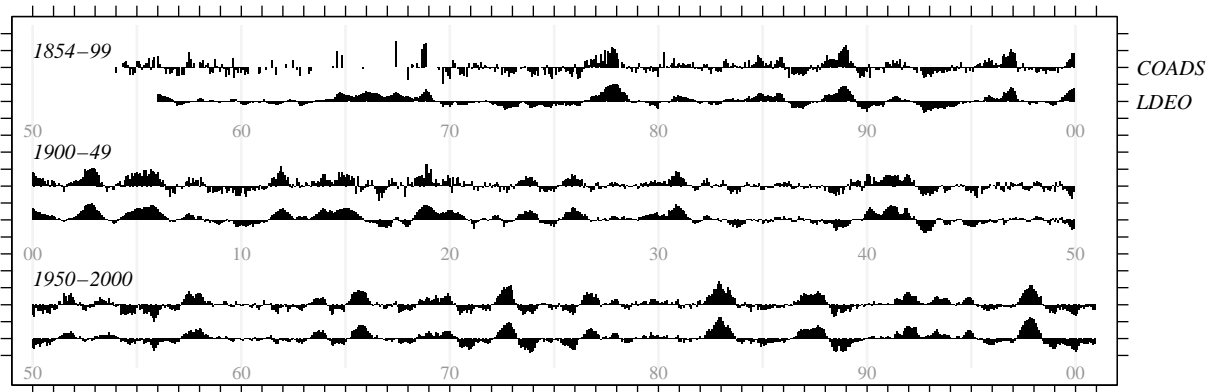


Figure 2

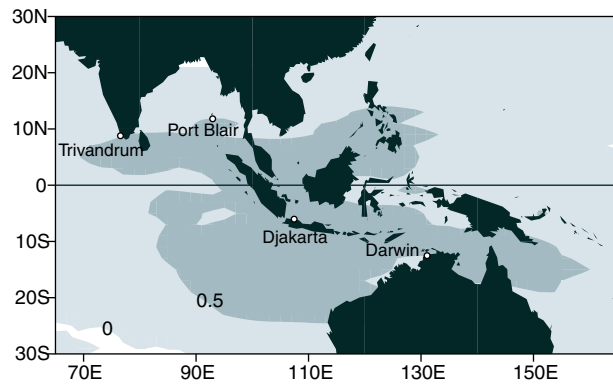


Figure 3

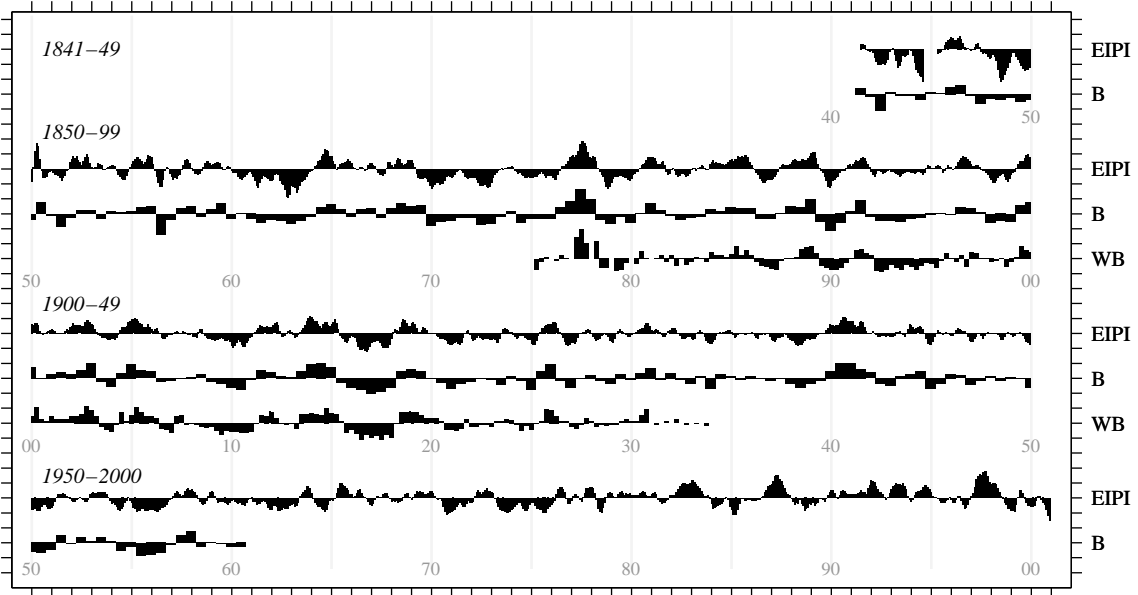


Figure 4

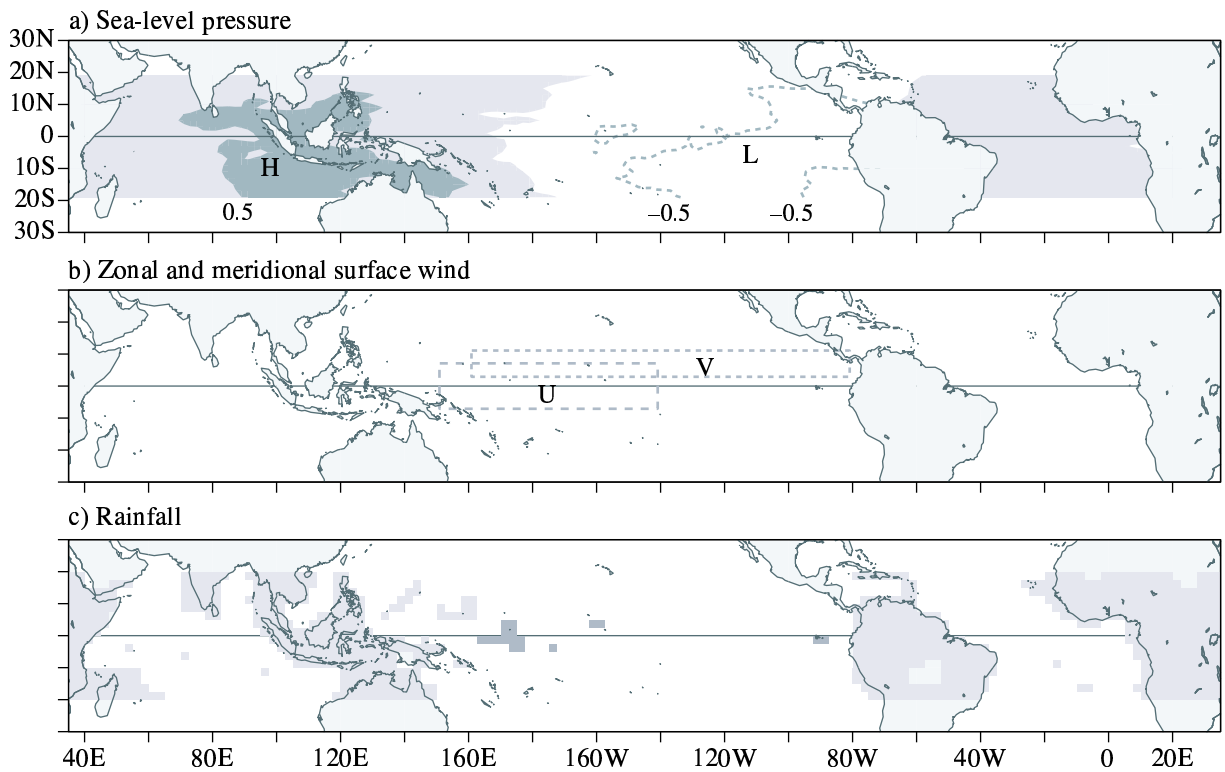


Figure 5

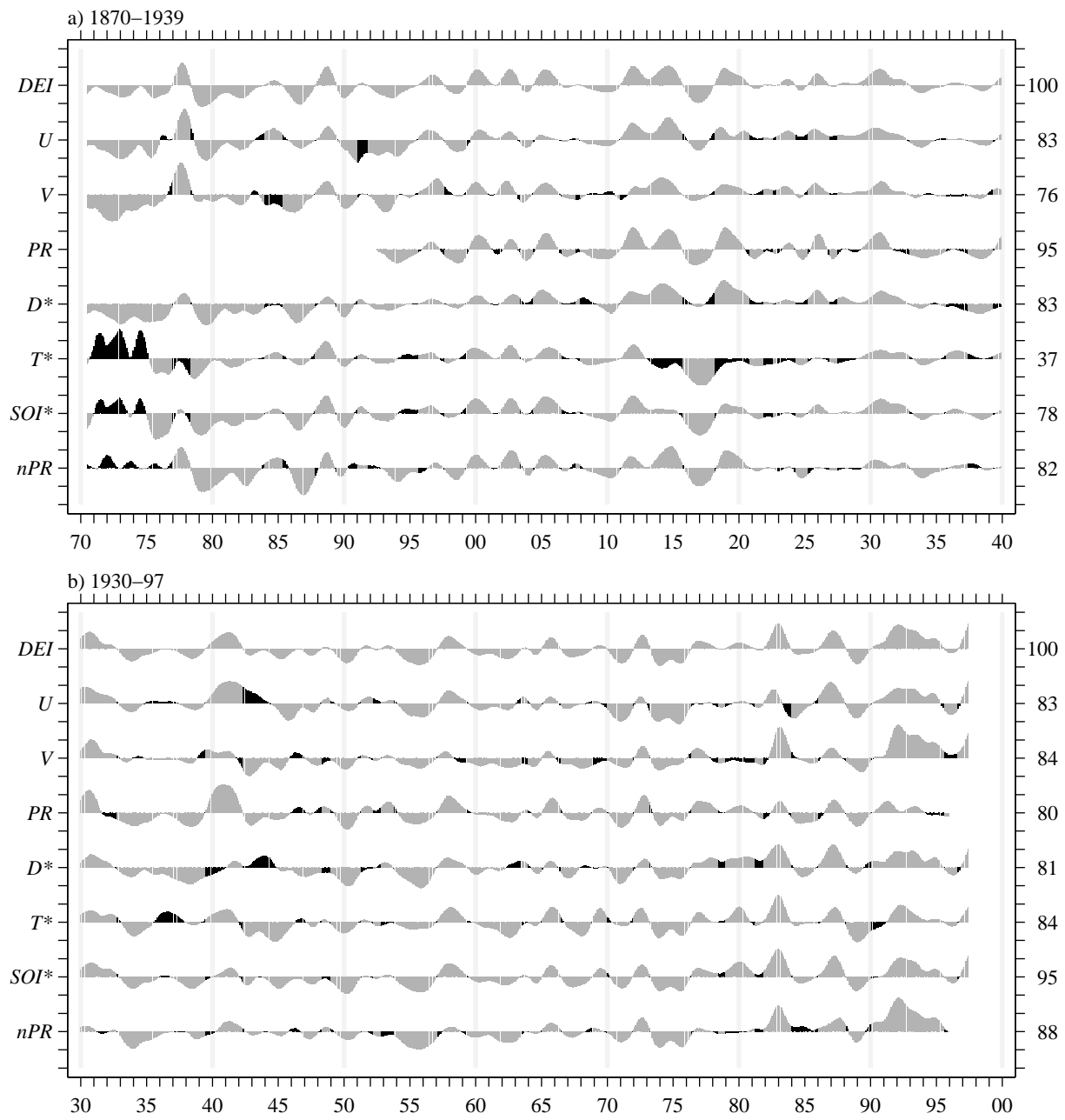


Figure 6

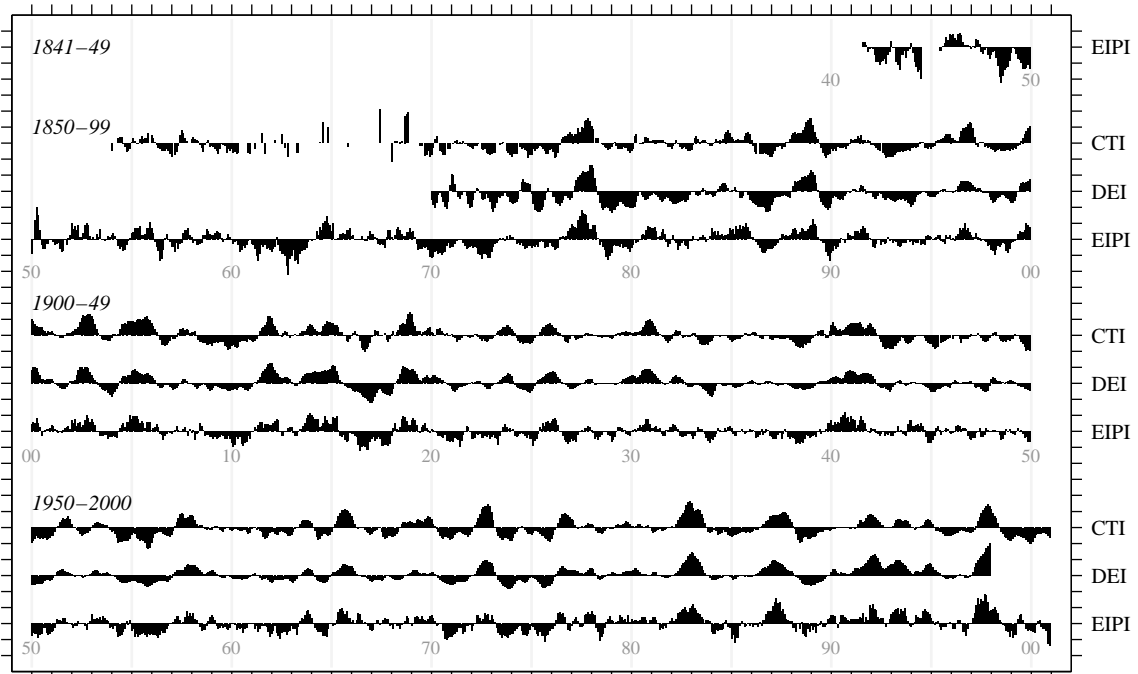


Figure 7

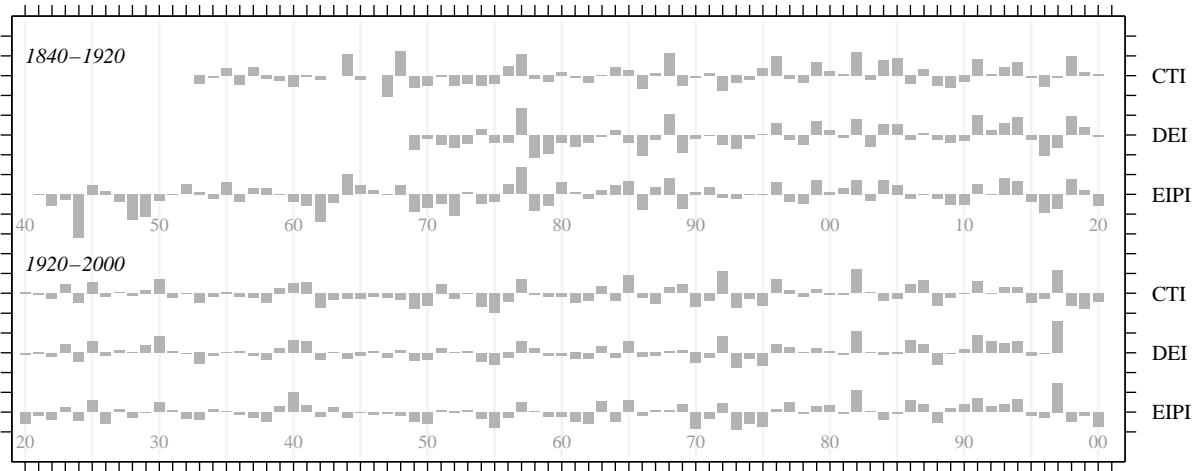


Figure 8

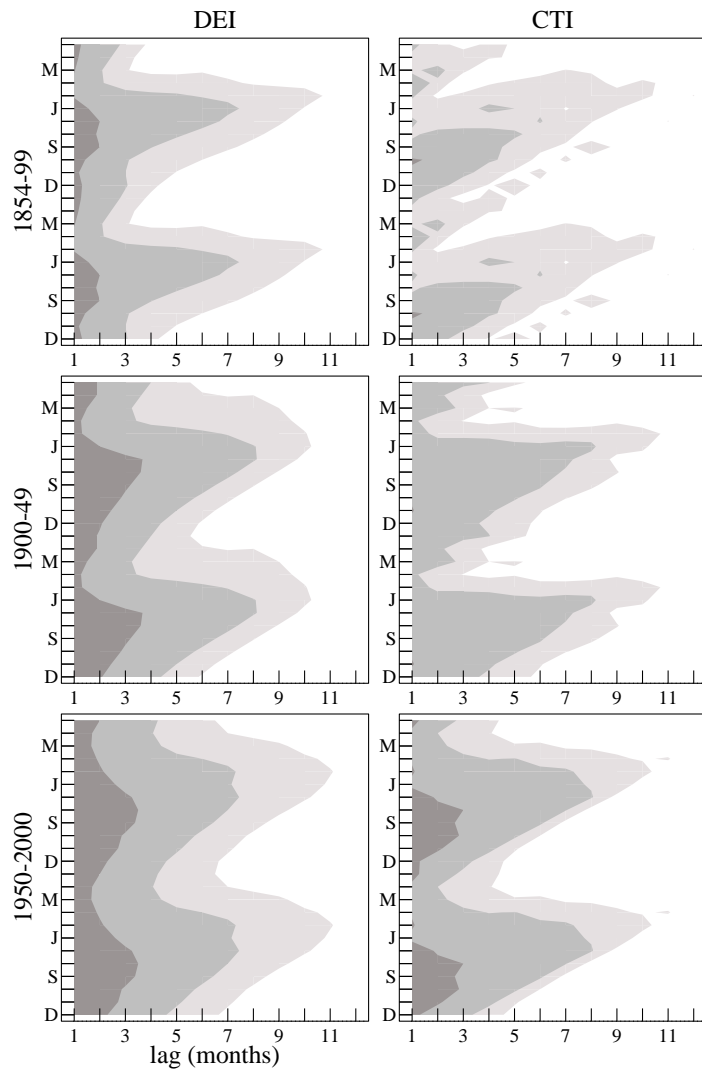


Figure 9

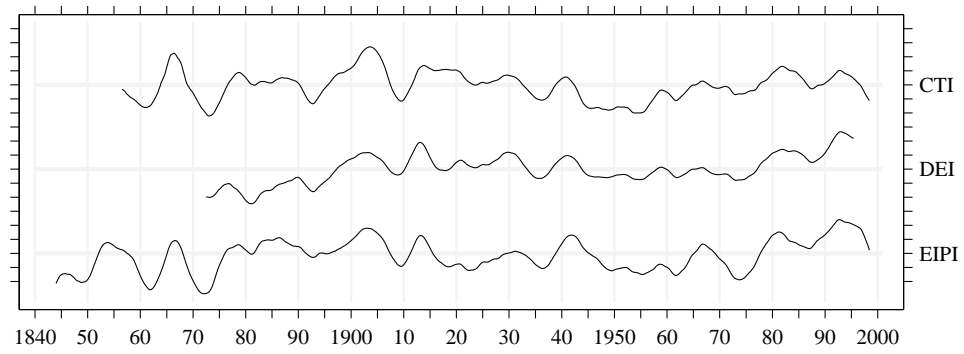


Figure 10

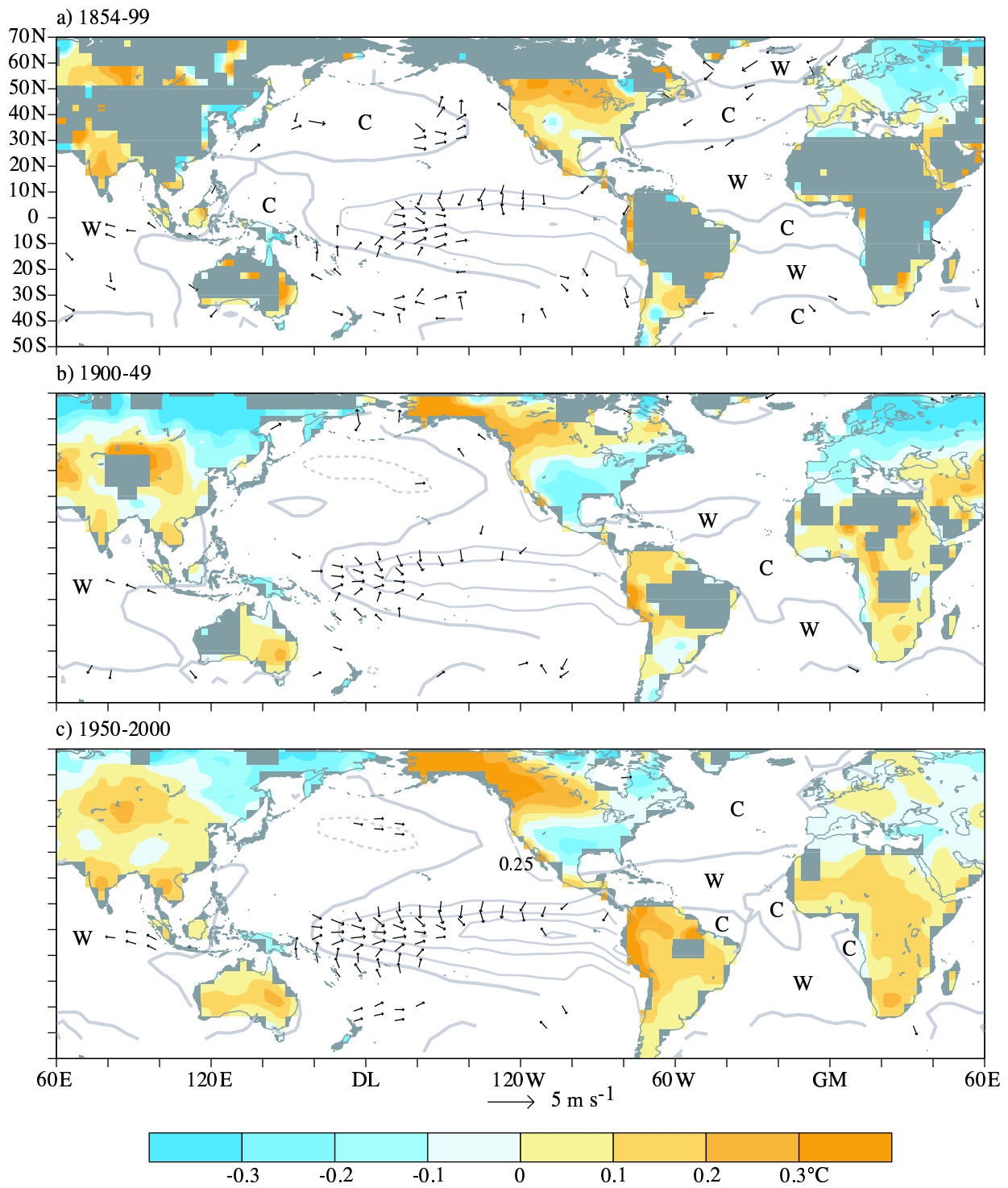


Figure 11

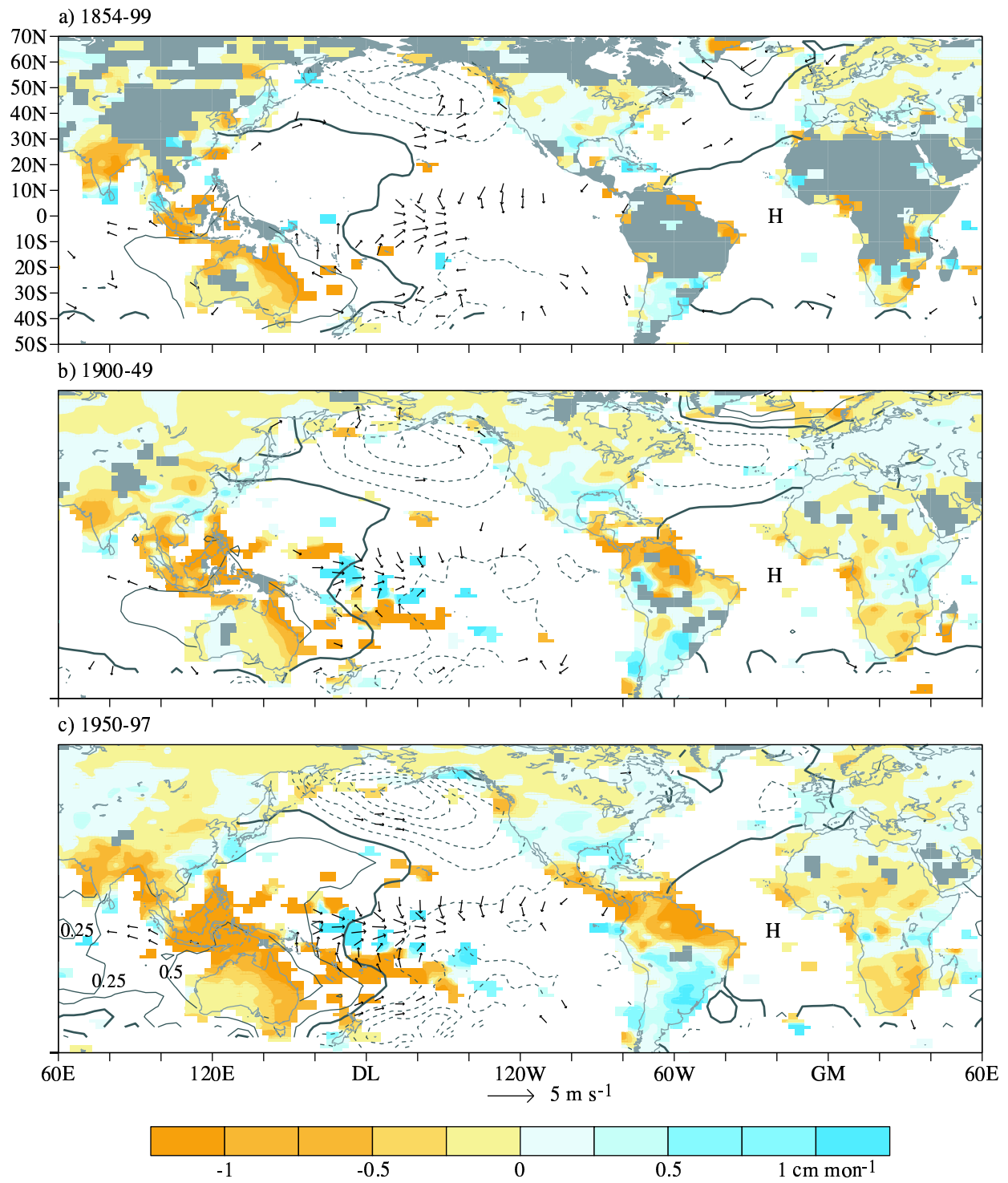


Figure 12

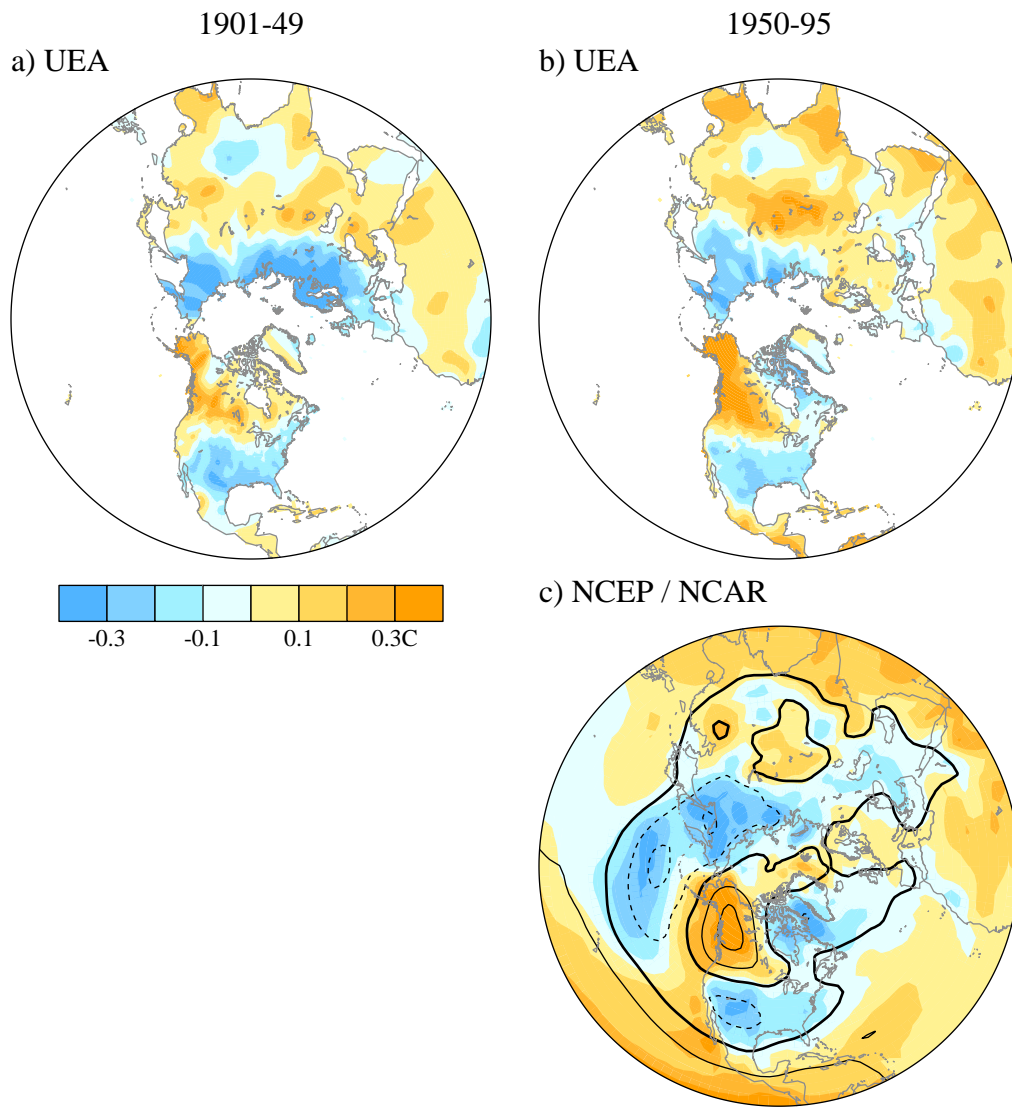


Figure 13

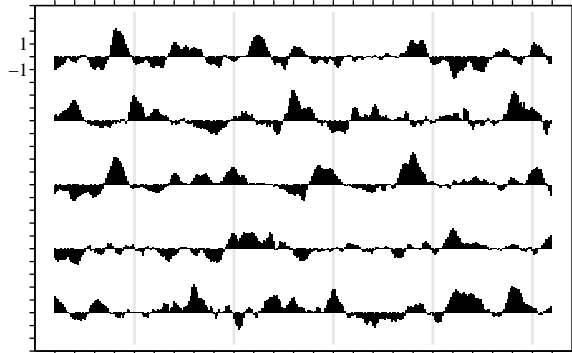


Figure 14

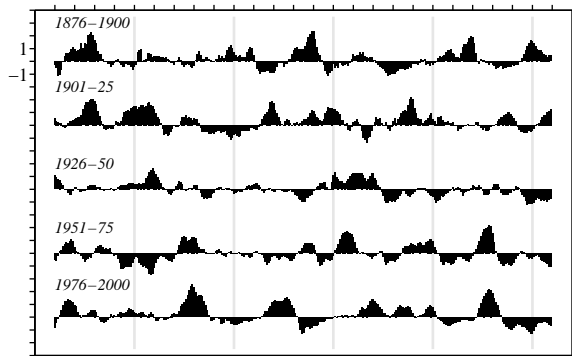


Figure 15